Please cite this article in press as: Rivera-Alba et al., Wiring Economy and Volume Exclusion Determine Neuronal Placement in the *Drosophila* Brain, Current Biology (2011), doi:10.1016/j.cub.2011.10.022

Current Biology *21*, 1–6, December 6, 2011 DOI 10.1016/j.cub.2011.10.022

Report

Wiring Economy and Volume Exclusion Determine Neuronal Placement in the *Drosophila* Brain

Marta Rivera-Alba,[1] Shiv N. Vitaladevuni,[2,4] Yuriy Mischenko,[2,5] Zhiyuan Lu,[3] Shin-ya Takemura,[2] Lou Scheffer,[2] Ian A. Meinertzhagen,[3] Dmitri B. Chklovskii,[2,*] and Gonzalo G. de Polavieja[1,*]

[1]Instituto Cajal, CSIC, Av. Doctor Arce 37, 28002 Madrid, Spain
[2]Janelia Farm Research Campus, Howard Hughes Medical Institute, VA 20147, USA
[3]Dalhousie University, Halifax, Nova Scotia B3H 3J5, Canada

Summary

Wiring economy has successfully explained the individual placement of neurons in simple nervous systems like that of *Caenorhabditis elegans* [1–3] and the locations of coarser structures like cortical areas in complex vertebrate brains [4]. However, it remains unclear whether wiring economy can explain the placement of individual neurons in brains larger than that of *C. elegans*. Indeed, given the greater number of neuronal interconnections in larger brains, simply minimizing the length of connections results in unrealistic configurations, with multiple neurons occupying the same position in space. Avoiding such configurations, or volume exclusion, repels neurons from each other, thus counteracting wiring economy. Here we test whether wiring economy together with volume exclusion can explain the placement of neurons in a module of the *Drosophila melanogaster* brain known as lamina cartridge [5–13]. We used newly developed techniques for semiautomated reconstruction from serial electron microscopy (EM) [14] to obtain the shapes of neurons, the location of synapses, and the resultant synaptic connectivity. We show that wiring length minimization and volume exclusion together can explain the structure of the lamina microcircuit. Therefore, even in brains larger than that of *C. elegans*, at least for some circuits, optimization can play an important role in individual neuron placement.

Results

Reconstruction from Electron Microscopy

Although the circuits of the fly's optic lamina have been a target of manual reconstruction using electron microscopy (EM) [6–8], testing wiring economy there requires a spatially more detailed description than is currently available. In particular, a "2D" wiring economy model like the one used in the next section also needs the sizes and positions of neurons in 2D and, more importantly, each branch of branched neurons must be represented separately in the wiring diagram. A "3D" wiring economy model would need, in addition to these data, further detail of neuron and synapse placement in the three spatial dimensions. To this end, we imaged 749 40 nm thick serial sections of the *Drosophila melanogaster* lamina by transmission EM (Figure 1A; see Experimental Procedures). Using a newly developed semiautomated EM reconstruction pipeline [14], we obtained the three-dimensional shapes of all neurons in a single lamina cartridge (Figures 1B and 1C; see also Figure S1 available online for the morphology of individual neurons).

To obtain the connectivity matrix, we identified synapses in the EM series and assigned them to presynaptic and postsynaptic neurons. We found 477 presynaptic terminals in the lamina cartridge, 57 of which were classified as uncertain because they met the required criteria only partially (Table S1; see Experimental Procedures for criteria). Each presynaptic terminal was apposed by several postsynaptic terminals with the total of 1,407 postsynaptic terminals, 94% of which could be assigned to identifiable neurons. The connectivity matrix (Figure 2A and Table S2; see Table S1 for a larger version with different neuronal subtypes and location of synapses in 3D) augments a previous manually obtained one [6, 7] (Figure S2), revealing a complex network structure, with approximately one third of the possible connections realized (Figure 2A). This complexity can be best seen in neuron-centric subnetworks including an individual neuron and all of its synaptic partners. The terminals of the photoreceptors are presynaptic to ten types of neurons and postsynaptic to seven (Figure 2B). Amacrine cells are interneurons with a rich connectivity structure (Figure 2C) that both receive and send synapses along the length of a cartridge. For some neurons, such as centrifugal cells C2 and C3, we found it helpful to include synaptic partners for both in the neuron-centric network (Figure 2D). C2 and C3 are mostly presynaptic in the lamina conveying feedback information from the medulla, the second optic neuropile. The large wide-field neurons Lawf span several cartridges and are mainly presynaptic but also receive information from the photoreceptor terminals and neuron C2 (Figure 2E). The large monopolar cells L1 and L2 that lie at the cartridge axis have similar connections, except that L1 is exclusively postsynaptic in the lamina, whereas L2 is presynaptic to the L4 complex comprising the local L4 axon and the two incoming collaterals of L4 from the neighboring cartridges, as well as to L5 (Figure 2F).

Wiring Economy in 2D

Insofar as the structure of the lamina cartridge varies little along its length (Figure 1B), we start by reducing a full 3D optimization problem to a simpler problem in 2D. Most neurons are columnar (Figure 1C), and have a simple structure, with a single cylindrical vertical axon and lateral branches to connect to other neurons (R1–R6, L1–L5, L4+x, L4−y, and three amacrine cell processes). The remaining lamina neurons include the 11 laterally directed varicose branches of Lawf cells. Thus, we represent each vertical process in 2D as a circle centered on the mean position of the neuron with a profile area given by the mean cross-sectional area of the neuron. Neurons having several vertical branches, such as medulla cell T1 (Figure S1H), and amacrine cell branch l (Aml) (Figure S1C), are represented in 2D using a circle for each branch, six for T1 and three for Aml. This makes a total of 38 neuronal elements represented

[4]Present address: Raytheon BBN Technologies, Cambridge, MA 02138, USA
[5]Present address: Toros University, 33140 Mersin, Turkey
*Correspondence: mitya@janelia.hhmi.org (D.B.C.), gonzalo.polavieja@cajal.csic.es (G.G.d.P.)

Please cite this article in press as: Rivera-Alba et al., Wiring Economy and Volume Exclusion Determine Neuronal Placement in the *Drosophila* Brain, Current Biology (2011), doi:10.1016/j.cub.2011.10.022

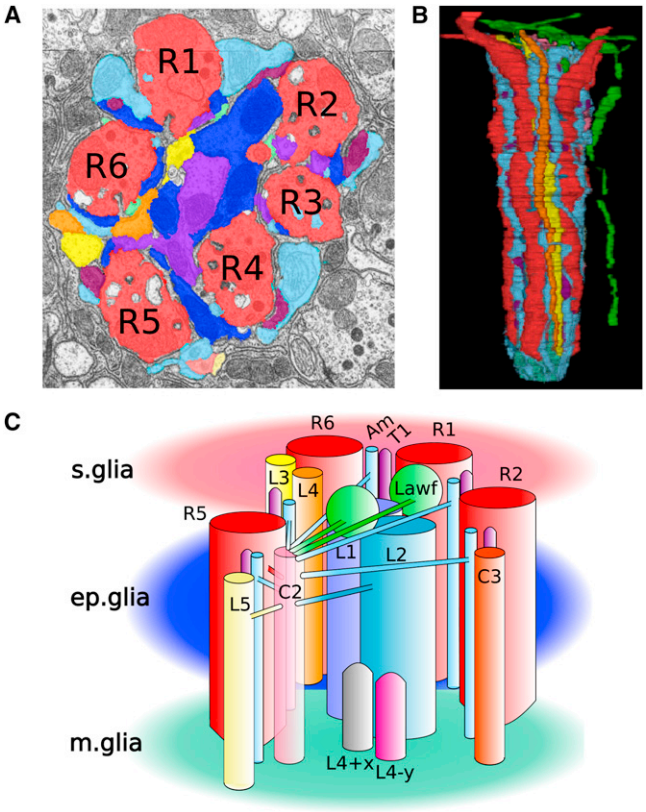

Figure 1. A Lamina Cartridge in *Drosophila melanogaster* Reconstructed in Three Dimensions from Serial Electron Microscopy Images

(A) Single electron microscopy (EM) image in which the cell profiles have been segmented and digitally labeled with different colors.

(B) Three-dimensional shapes of the neurons in the reconstructed cartridge; see Figure S1 for shapes of individual neurons.

(C) Schematic version of (B). Neurons connect with lateral branches, here illustrated for neuron C2. The following abbreviations are used: R1–R6, photoreceptors terminals 1 to 6; L1–L5, lamina monopolar cells 1 to 5; L4+x and L4−y, incoming L4 collaterals from the two neighboring anterior cartridges along the +x and −y axes, respectively; Am, amacrine cells; T1, T medulla neuron 1; C2 and C3, centrifugal medulla neurons C2 and C3; Lawf, lamina wide-field cells; ep. Glia, epithelial glia; s. glia, satellite glia; m. glia, marginal glia. To enable their visualization, we show only four of the six photoreceptors, five of the six T1 branches, and two of the 11 Lawf branches.

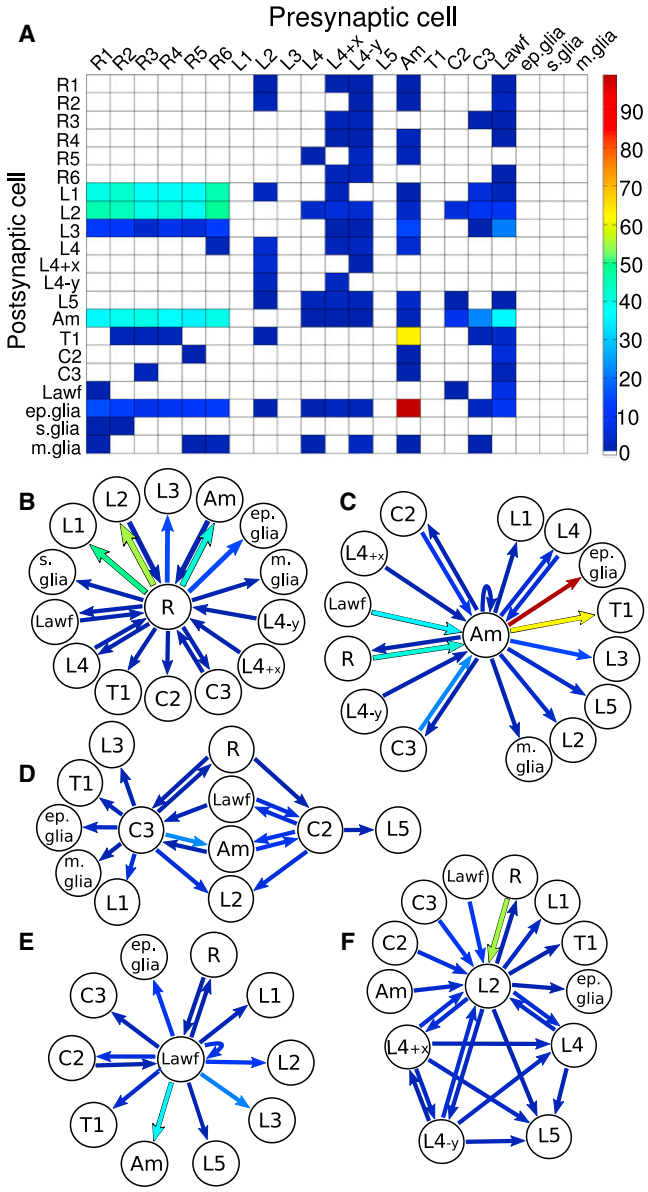

Figure 2. Connectivity in the Lamina Cartridge

(A) Connectivity matrix; see Table S1 for an extended matrix including neuronal subtypes and Table S2 for a numerical version. Hotter colors indicate a larger number of synapses.

(B–F) Representation of neurons and connecting neighbors for a photoreceptor (B), an amacrine neuron (C), centrifugal neurons C2 and C3 (D), a large wide-field neuron Lawf (E), and large monopolar cell L2 (F).

in 2D as circles of different sizes. Although some of these elements correspond to neurons that derive from and thus "belong" to another cartridge, these neurons all enter through the proximal base of the cartridge and so do not affect neuronal placement in 2D.

We next used this two-dimensional version of the actual data to test whether it corresponds to a configuration with a low total length of lateral connecting branches (see wiring cost in equation 1 of Supplemental Experimental Procedures). We kept the same set of neuron positions (the centers of the circles in 2D) fixed but permuted the neurons to produce random configurations. We found that the experimental configuration had wiring costs lower than one million random configurations, and by extrapolating the distribution of wiring costs of the random configurations, we obtained $p < 10^{-7}$ (Figure S3A).

As a second approach to test for wiring economy of the lamina microcircuit, we minimized wiring cost while varying neuron locations (the centers of the circles in 2D) and compared optimal configurations with the one observed experimentally. As wiring economy alone would only produce the trivial solution in which all neurons overlap each other, we also included volume exclusion (Figure 3A; see equation 2 in Supplemental Experimental Procedures and Table S3 and Table S4 for connectivity and neuronal radii and neuron positions, respectively). For short distances (less than the sum of the radii of the two neurons), the cost consisted of a soft repulsion term modeling volume exclusion by neurons. For larger distances, the cost is due to the wiring length of lateral connecting branches. This was modeled as proportional to the distance between the two neurons and with slope

Please cite this article in press as: Rivera-Alba et al., Wiring Economy and Volume Exclusion Determine Neuronal Placement in the *Drosophila* Brain, Current Biology (2011), doi:10.1016/j.cub.2011.10.022

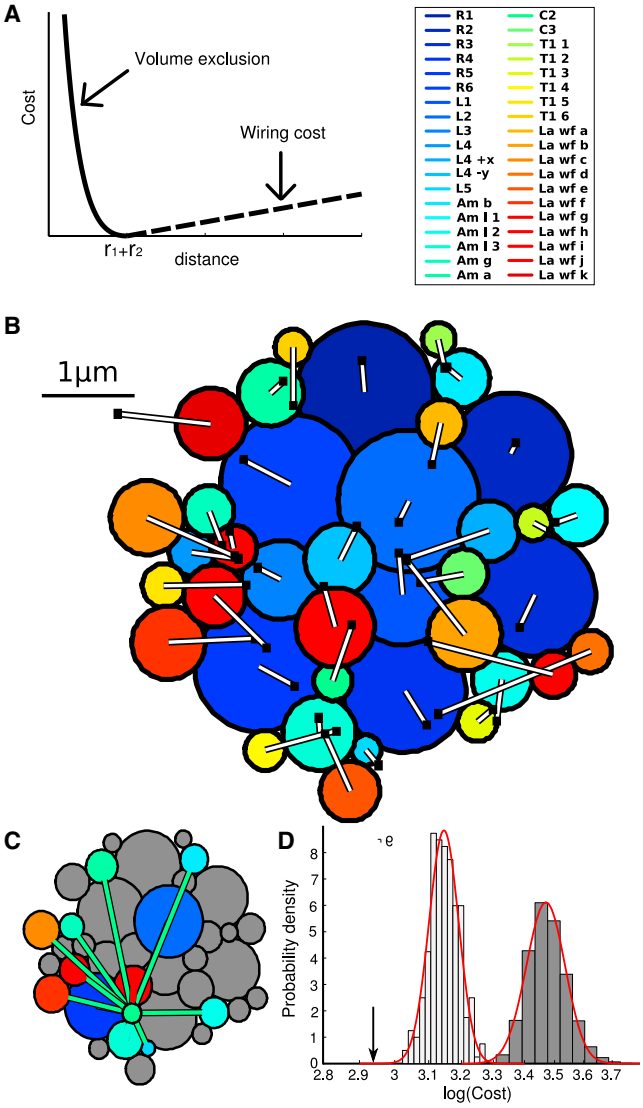

Figure 3. Wiring Economy in 2D

(A) Pairwise cost between two neurons used to model soft volume exclusion for short distances and wiring length cost for distances larger than the sum of the radii of the two profiles of partner neurons. r_i is the radius of the i neuron.

(B) Configuration of the lowest cost found by simulated annealing (SA) when the initial configuration is the actual one. White lines connect to actual positions marked by black squares.

(C) The configuration computed in (B) is nontrivial because it includes both connections to close and distant neurons, illustrated for neuron C2.

(D) The actual cost of the computed configuration in (B) (arrow) is significantly lower than random configurations obtained by permuting large neuron profiles with other large neuron profiles, or small profiles with small (dark gray histogram), and 240 other converged configurations found by SA using random initial configurations (white histogram).

given by the number of synaptic connections between them. Because we had 38 neuronal elements, the total cost was a sum of 703 pairwise cost functions like the one shown in Figure 3A, each using the actual connections and the actual radii of the two corresponding neurons.

To find low-cost configurations for the 38 neuronal elements, we resorted to a heuristic method known as simulated annealing (SA) [15], which is designed for solutions to avoid trivial local minima of high cost. We first used SA to test whether the actual configuration is close to a minimum of the cost function. For this, we used the actual location of neurons in the lamina as the initial condition for SA calculations and found the configuration in Figure 3B as the one with the lowest cost. The centers of the circles in Figure 3B are at the computed positions, and their profile areas are drawn to the actual areas. For comparison with the actual system, we plotted white bars connecting each computed neuron location to the actual location (Figure 3B, black square). The mean distance between the computed and actual neuron is 0.56 μm, relatively small compared with the value of 1.9 ± 0.1 μm of randomized configurations obtained by permuting the neurons. Also, we note that the computed configuration is nontrivial because neurons not only connect to close neighbors but also to distant neurons, as illustrated in Figure 3C for neuron C2.

To understand the significance of the computed configuration in Figure 3B, we performed several control calculations. First we checked that this configuration is at least at a local minimum of the cost by showing that small deviations of any neuron increased the cost (Figure S3B). We also checked that the result does not depend on the functional form of the "soft repulsion" term of the cost (Figure S3C).

Having established that the actual configuration is close to a minimum of the cost function, we note that SA cannot guarantee converging to the global minimum in practice. Therefore, we needed to determine whether this minimum was special in its value of cost. First, we compared the cost of this minimum with the cost of one million configurations obtained by randomly exchanging large (small) neurons with large (small ones) to avoid repulsion costs that were too large (Figure 3D, dark gray histogram). None of the randomized configurations had a lower cost, and by extrapolating a fit to the histogram of costs for these random configurations, we found that $p < 10^{-16}$. More importantly, we tested whether the local minimum found is also in a configuration of cost lower than other minima of the surface cost and not only compared to random configurations. For this test, we ran 240 SA simulations with initial configurations chosen randomly and found that they all converged upon configurations having larger costs and that were further away from the actual experimental configuration, and by extrapolation we found a large significance of $p < 10^{-5}$ (Figure 3D, white histogram). The actual configuration of neurons in a lamina cartridge is thus close to a minimum cost configuration that is significantly lower in its cost compared with the rest of cost surface and other minima.

In addition to the foregoing tests, we checked that the deviations from the minimum-cost placement follow the structure predicted to exist in wiring economy solutions in the presence of other unknown factors [3] (Figures S3D and S3E).

Connectivity and Size as Opposing Forces in the Lamina

Our modeling approach included two types of observational data: the actual connectivity matrix and the sizes of the neurons. To better understand the role these two factors play in the low cost configuration, we manipulated them independently (Figure 4A). First, we manipulated the radii of the profiles representing axons (Figure 4A, green line). Errors increased when forcing all radii to be equal to the mean profile area ("homogeneous case") or when assigning large radii to neurons that in reality had small radii, and vice versa ("inverted case"). The concerted effect of wiring economy and volume exclusion pushes neurons with the largest profile areas to the periphery of the cartridge, so as to prevent their

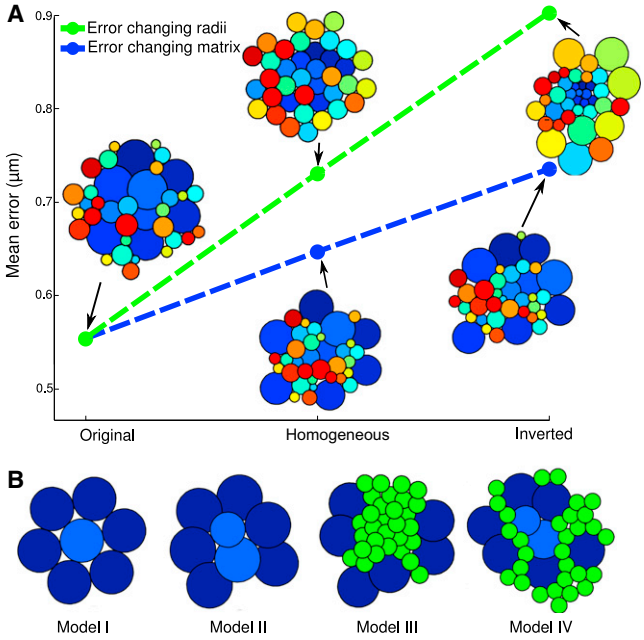

Figure 4. Roles of Connectivity and Axon Sizes

(A) Error of six wiring economy configurations with respect to the experimental configuration. The green line includes two manipulations of neuronal radii, one forcing all neurons to have the same size (homogeneous case) and another one in which the larger neurons are modeled as the smaller ones and vice versa (the inverted case). The blue line includes two manipulations of the connectivity matrix, one making all connecting neurons use the same number of synapses (homogeneous case) and the other one in which neuron pairs with the largest number of synapses are modeled as the ones with the smaller numbers (inverted case).

(B) Wiring economy in simplified models. Model I shows wiring economy configuration in a simplified model in which the dark blue neurons (photoreceptor terminals) are connected only to one light blue one (L1 or L2). Model II shows wiring economy configuration including now both L1 and L2 neurons. Model III shows wiring economy configuration with photoreceptor terminals and 30 smaller neurons having a random connectivity matrix. Model IV shows same as model III but including neurons L1 and L2.

obstructing the paths of neurites extending between connecting neurons.

We also tested the importance of the connectivity matrix (Figure 4A, blue line). We modified the number of synapses connecting pairs of neurons, leaving the topology of connections intact. In the original configuration, we used the real numbers, in which there are more synapses from all R1–R6 photoreceptors to L1 and L2 than smaller neurons have between any two neuron partners. This difference implies, together with wiring economy, that L1 and L2 should be close to all the photoreceptor terminals, in the only arrangement possible, at the center of the cartridge. This tendency is reduced when we make all the numbers of synapses between neurons equal in the homogeneous case or when assigning fewer synapses from photoreceptor terminals to L1 and L2 than those between the neurons with smaller axons in the inverted case.

Synapse number and neuron size thus play opposing roles in the wiring economy of the lamina cartridge. The actual values of synapses observed (with most from the photoreceptor terminals to L1 and L2) imply that the neurons with smaller axons should be located preferentially around the periphery of the cartridge because wiring economy dictates that L1 and L2 should occupy the cartridge axis. The real sizes and the concerted effects of wiring economy and volume exclusion require, by contrast, the neurons with larger axons to occupy peripheral positions. The actual arrangement observed is the result of a balance between these two opposing effects.

Models with Simplified Connectivities

The eight neurons with the largest caliber axons (six photoreceptor terminals R1–R6, L1 and L2) stand out as forming the largest number of synapses (Figure 2A). Including only L1 or L2 and the photoreceptor terminals, the minimum cost configuration has a hexagonal shape (model I, Figure 4B), one that is distorted when including both L1 and L2 (model II, Figure 4B). The neurons with smaller caliber axons have a more complex structure in the experimental connectivity matrix that we modeled in a very simple way by a random matrix having a mean connectivity as in the actual system (four synapses for connecting neurons and a probability of connection of 0.2), whereas photoreceptor terminals to L1 and L2 each have 42 synapses. Wiring length minimization with volume exclusion for the six photoreceptors and the small neurons (without L1 and L2) predict the structure in model III of Figure 4B, with all large objects around the periphery of the cartridge cross-section. Including all neurons, the minimum cost configuration we found is shown in model IV of Figure 4B. In this case, the axons of L1 and L2, which make many connections with the six photoreceptor terminals, lie at the center of the cartridge, along its axis, because other configurations would have larger values of total wiring length. This configuration captures some of the basic features of the biological system, even though no one-to-one correspondence between the axon locations of modeled and real neurons is seen for the neurons with small caliber axons due to differences in the simplified connectivity matrix.

Wiring Economy in 3D

In the real lamina, the 2D network connectivity changes with the depth of the lamina, down the length of the cartridge, mainly because some neurons such as C2 or L4 are synaptic only at certain depths. In principle, one can build a 3D model with each neuron represented as a collection of n connected volumes, making the number of elements in the cartridge 38 n. To make computations practicable, we used n = 3, a number that captures the main changes in 2D connectivity down the depth of the cartridge. The model thus used an overall connectivity consisting of 2D layers linked by common neurons (Table S5), the axon sizes of neurons in the three layers (Table S6). The 3D model also included a cost in the z direction to take into account the rigidity of neurons (Supplemental Experimental Procedures). SA found the wiring economy configuration in Figure 5, plotted separately for distal (Figure 5A), central (Figure 5B), and proximal depths (Figure 5C). Wiring economy and volume exclusion can thus explain closely the 3D structure with low errors (0.5, 0.22, and 0.23 μm for distal, central, and proximal configurations, respectively).

Discussion

We have found that a lamina cartridge in the fly's brain, a microcircuit of 38 neuronal elements that repeats 800 times, can be explained in detail by the principles of wiring economy [1–4, 16–25] and volume exclusion. The model used several simplifying assumptions. First, wiring cost was proportional

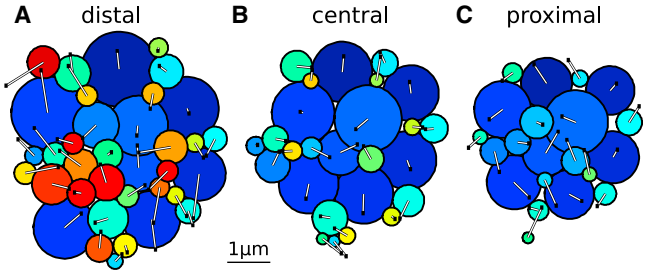

Figure 5. Wiring Economy in 3D

From a wiring economy computation in 3D, configurations in distal (A), central (B), and proximal (C) regions of the cartridge. The neurons are placed in their computed positions with the experimental areas. Lines connect the computed to the observed positions.

to the number of synapses between two given neurons. In effect this assumes that there is the same number of synapses per wire for each neuron. However, we expect only minor improvements when adding different values for each neuron because even a binary connectivity matrix explains the structure well (Figure 4A, homogeneous case on blue line). This agreement shows that wiring economy, given the actual network topology and the neurons' axon calibers, are the main determinants of cartridge structure. A second simplifying assumption was to model volume exclusion as a repulsive potential. An explicit consideration of neuronal deformations would dramatically increase the space available for possible configurations and would make the problem computationally intractable. Furthermore, our wiring cost function assumes that wires follow straight lines connecting partner neurons. Again, considering more realistic tortuous paths would dramatically increase the complexity of computations required. This modeling approach to include both wiring cost and volume and its assumptions should be of value to many different neuronal systems. Finally, we did not take into account gap junctions because these are not clearly visible in our EM images and have not been annotated. Interestingly, gap junctions are known to exist between neighboring photoreceptor terminals [26] and have recently been reported, although not localized, between neurons L1 and L2 [27]. In our model's optimal placement, the axons of these two cells are already abut each other, meaning that the inclusion of gap junctions between them is not going to affect the wiring economy solution.

A complete circuit diagram with the level of detail and accuracy like the one presented here should also allow for more detailed developmental, functional, and behavioral studies. The circuit diagram should allow for a better targeting of neurons for circuit manipulation to test functional principles [9–13], as well as to constrain theoretical models. Further, it should allow for more detailed tests of other basic principles like information transfer and energy optimization [6, 28–31]. In particular, wide variation of cross-sectional areas among different neurons could help address these relationships [32]. The wiring diagram should also allow testing for whether basic principles like wiring economy are embedded in developmental programs or emerge as a result of natural selection of the adult brains. Specifically, experimental manipulations of the connectivity, together with EM reconstructions and the analysis presented here, should help determine whether processes in development [33] automatically allow for a match between connectivity and wiring economy.

Experimental Procedures

All images are from the same transmission electron microscopy series of the dorsal side of the left eye from a 9-day-old female Oregon R *Drosophila melanogaster*. After imaging, we applied a semiautomatic reconstruction protocol developed at Janelia Farm Research Campus [5] to those images containing our cartridge of interest. The synapses were manually annotated after the reconstruction using the software Raveler (D. Olbris, P. Winston, and D.B. Chklovskii). Three criteria were required to validate the presence of a synapse: the existence of a T-bar ribbon in the presynaptic terminal, the existence of surrounding vesicles in the presynaptic terminal, and the clear apposition of postsynaptic profiles, either dendrites or axons. The cost function used for modeling included a term for wiring length cost and a repulsion term for volume exclusion, and configurations of minimum cost were found by SA.

See Supplemental Experimental Procedures for details of all procedures.

Supplemental Information

Supplemental Information includes three figures, six tables, and Supplemental Experimental Procedures and can be found with this article online at doi:10.1016/j.cub.2011.10.022.

Acknowledgments

We are grateful to Richard Fetter for assistance in EM imaging and Janelia FlyEM Project Team and Aljoshcha Nern for helpful comparisons with images from Gal4-driven expression of green fluorescent protein in lamina cells. M.R.-A. acknowledges a Formación del Personal de Investigación (FPI) fellowship from Ministerio de Ciencia e Innovación (MICINN) and support from the Janelia Farm Research Campus (JFRC) (Howard Hughes Medical Institute [HHMI]) visitor program; G.G.d.P. acknowledges funding by MICINN (Spain) as Plan Nacional, including a FPI fellowship and as partners of the ERASysBio+ initiative supported under the EU ERA-NET Plus scheme in FP7, and support from the JFRC (HHMI) visitor program. I.A.M. also acknowledges support from the JFRC (HHMI) visitor program.

Received: September 9, 2011
Revised: October 11, 2011
Accepted: October 17, 2011
Published online: November 23, 2011

References

1. Chen, B.L., Hall, D.H., and Chklovskii, D.B. (2006). Wiring optimization can relate neuronal structure and function. Proc. Natl. Acad. Sci. USA *103*, 4723–4728.
2. Pérez-Escudero, A., and de Polavieja, G.G. (2007). Optimally wired subnetwork determines neuroanatomy of *Caenorhabditis elegans*. Proc. Natl. Acad. Sci. USA *104*, 17180–17185.
3. Pérez-Escudero, A., Rivera-Alba, M., and de Polavieja, G.G. (2009). Structure of deviations from optimality in biological systems. Proc. Natl. Acad. Sci. USA *106*, 20544–20549.
4. Klyachko, V.A., and Stevens, C.F. (2003). Connectivity optimization and the positioning of cortical areas. Proc. Natl. Acad. Sci. USA *100*, 7937–7941.
5. Laughlin, S.L. (1981). A simple coding procedure enhances a neuron's information capacity. Z. Naturforsch., C, Biosci. *36*, 910–912.
6. Meinertzhagen, I.A., and O'Neil, S.D. (1991). Synaptic organization of columnar elements in the lamina of the wild type in *Drosophila melanogaster*. J. Comp. Neurol. *305*, 232–263.
7. Meinertzhagen, I.A., and Sorra, K.E. (2001). Synaptic organization in the fly's optic lamina: few cells, many synapses and divergent microcircuits. Prog. Brain Res. *131*, 53–69.
8. Takemura, S.Y., Lu, Z., and Meinertzhagen, I.A. (2008). Synaptic circuits of the *Drosophila* optic lobe: the input terminals to the medulla. J. Comp. Neurol. *509*, 493–513.
9. Zhu, Y., Nern, A., Zipursky, S.L., and Frye, M.A. (2009). Peripheral visual circuits functionally segregate motion and phototaxis behaviors in the fly. Curr. Biol. *19*, 613–619.
10. Zheng, L., de Polavieja, G.G., Wolfram, V., Asyali, M.H., Hardie, R.C., and Juusola, M. (2006). Feedback network controls photoreceptor output at the layer of first visual synapses in *Drosophila*. J. Gen. Physiol. *127*, 495–510.

11. Rister, J., Pauls, D., Schnell, B., Ting, C.Y., Lee, C.H., Sinakevitch, I., Morante, J., Strausfeld, N.J., Ito, K., and Heisenberg, M. (2007). Dissection of the peripheral motion channel in the visual system of *Drosophila melanogaster*. Neuron *56*, 155–170.
12. Eichner, H., Joesch, M., Schnell, B., Reiff, D.F., and Borst, A. (2011). Internal structure of the fly elementary motion detector. Neuron *70*, 1155–1164.
13. Clark, D.A., Bursztyn, L., Horowitz, M.A., Schnitzer, M.J., and Clandinin, T.R. (2011). Defining the computational structure of the motion detector in *Drosophila*. Neuron *70*, 1165–1177.
14. Chklovskii, D.B., Vitaladevuni, S., and Scheffer, L.K. (2010). Semi-automated reconstruction of neural circuits using electron microscopy. Curr. Opin. Neurobiol. *20*, 667–675.
15. Kirkpatrick, S., Gelatt, C.D.J., Jr., and Vecchi, M.P. (1983). Optimization by simulated annealing. Science *220*, 671–680.
16. Ramón y Cajal, S. (1899). Textura del Sistema Nervioso del Hombre y los Vertebrados (Texture of the Nervous System of Man and Vertebrates) (New York: Springer-Verlag).
17. Mitchison, G. (1991). Neuronal branching patterns and the economy of cortical wiring. Proc. R. Soc. Lond. B Biol. Sci. *245*, 151–158.
18. Cherniak, C. (1992). Local optimization of neuron arbors. Biol. Cybern. *66*, 503–510.
19. Chklovskii, D.B., Schikorski, T., and Stevens, C.F. (2002). Wiring optimization in cortical circuits. Neuron *34*, 341–347.
20. Cherniak, C., Mokhtarzada, Z., Rodriguez-Esteban, R., and Changizi, K. (2004). Connectivity optimization and the position of cortical areas. Proc. Natl. Acad. Sci. USA *101*, 1081–1086.
21. Buzsáki, G., Geisler, C., Henze, D.A., and Wang, X.J. (2004). Interneuron Diversity series: Circuit complexity and axon wiring economy of cortical interneurons. Trends Neurosci. *27*, 186–193.
22. Chklovskii, D.B. (2004). Synaptic connectivity and neuronal morphology: two sides of the same coin. Neuron *43*, 609–617.
23. Chklovskii, D.B. (2004). Exact solution for the optimal neuronal layout problem. Neural Comput. *16*, 2067–2078.
24. Chklovskii, D.B., and Koulakov, A.A. (2004). Maps in the brain: what can we learn from them? Annu. Rev. Neurosci. *27*, 369–392.
25. Cuntz, H., Forstner, F., Borst, A., and Häusser, M. (2010). One rule to grow them all: a general theory of neuronal branching and its practical application. PLoS Comput. Biol. *6*, e1000877.
26. Ribi, W.A. (1978). Gap junctions coupling photoreceptor axons in the first optic ganglion of the fly. Cell Tissue Res. *195*, 299–308.
27. Joesch, M., Schnell, B., Raghu, S.V., Reiff, D.F., and Borst, A. (2010). ON and OFF pathways in *Drosophila* motion vision. Nature *468*, 300–304.
28. Balasubramanian, V., Kimber, D., and Berry, M.J., 2nd. (2001). Metabolically efficient information processing. Neural Comput. *13*, 799–815.
29. de Polavieja, G.G. (2002). Errors drive the evolution of biological signalling to costly codes. J. Theor. Biol. *214*, 657–664.
30. Balasubramanian, V., and Berry, M.J., 2nd. (2002). A test of metabolically efficient coding in the retina. Network *13*, 531–552.
31. Niven, J.E., Anderson, J.C., and Laughlin, S.B. (2007). Fly photoreceptors demonstrate energy-information trade-offs in neural coding. PLoS Biol. *5*, e116.
32. Perge, J.A., Koch, K., Miller, R., Sterling, P., and Balasubramanian, V. (2009). How the optic nerve allocates space, energy capacity, and information. J. Neurosci. *29*, 7917–7928.
33. Prakash, S., Caldwell, J.C., Eberl, D.F., and Clandinin, T.R. (2005). *Drosophila* N-cadherin mediates an attractive interaction between photoreceptor axons and their targets. Nat. Neurosci. *8*, 443–450.